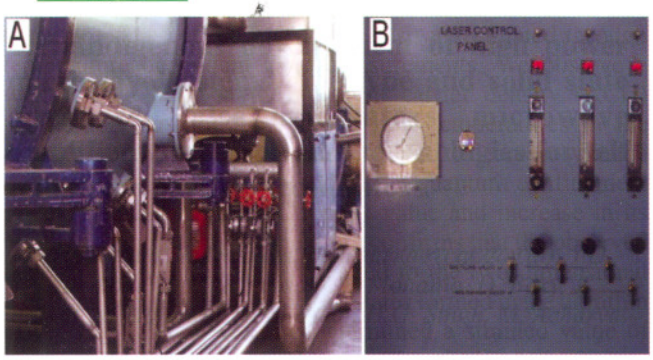

Fig.L.2.2: (A) Secondary coolant circuit and (B) gas purging controller.

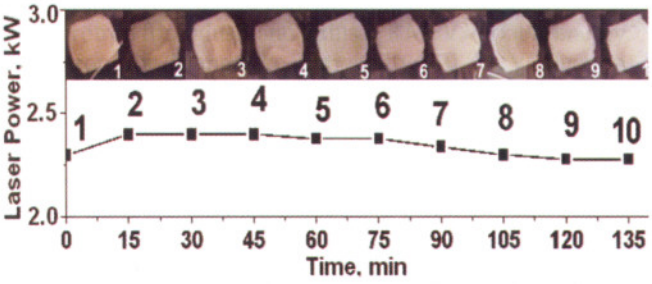

Fig.L.7.3: Variation of laser power & beam shape during laser operation in single filling/isolation mode.

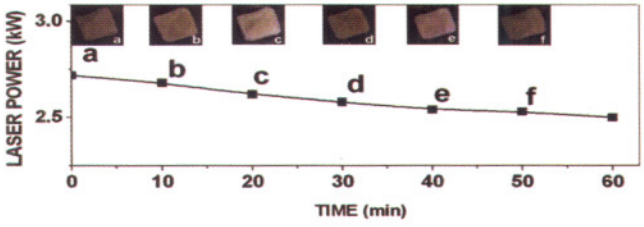

Fig.L.7.4: Variation of laser power and beam shape during laser operation in purging mode.

The performance of renovated laser system has been tested. The transparent glow discharge was achieved and a total 63 kW input power was dissipated in 2 x 1 m long discharge zone with inter electrode gap of 35 mm. The optimum gas mixture was: 2 mbar of CO_2, 14 mbar of N_2 and 34 mbar of He. Laser system delivered maximum output power of 5.8 kW with electro-optic efficiency of 14%. Figs. L.7.3 and L.7.4 present variation of output laser power and beam shape and size during laser operation in single filling/isolation and optimized purging modes, respectively. The maximum variation in laser power during 135 min. long laser operation in purging mode was about ± 3%. The shape and size of laser beam remained almost unchanged during the operation of the laser system.

Reported by:
Harish Kumar (harishk@rrcat.gov.in)

L.8: Effect of volume fraction on the third-and fifth-order nonlinearity of nanoplatelet colloids

Transient absorption measurements can be used to study the carrier dynamics as well as the nonlinearity of a material. Using this technique, we have measured the effect of volume fraction of silver in water, on the imaginary part of third- and fifth-order nonlinearities in silver nanoplatelet colloid.

The optical response of a colloidal material formed by dilutely dispersed metal nanoparticles in a host depends on the dielectric constants of the host as well as the nanoparticle. When the nonlinear response of the material is instantaneous, a generalized Maxwell-Garnett theory with T-matrix formalism can be used to understand its various nonlinear susceptibilities. Experimental measurement on scaling of the nonlinear optical coefficients with the volume fraction is used to validate the theoretical results. However, for materials with slow response there are no experimental and theoretical investigations. In metal the hot electron contribution to the nonlinearity is slow since it takes about 350 fs for the electrons to thermalize. Our measurements were performed using a 100 fs pulses delivered by a Ti:Sapphire laser operated at 800 nm wavelength. Thus the pulse width used in the experiment was lower than the thermaization time of electrons. The silver nanoplatelets colloid studied has localized surface plasmon resonance (LSPR) at 787 nm and 331 nm.

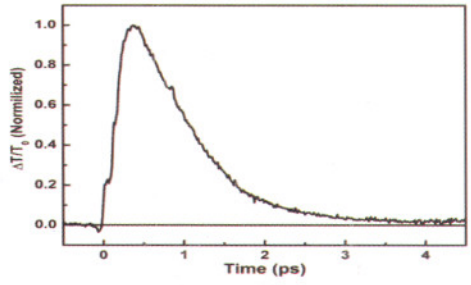

Fig. L.8.1. The time dependent transimitivity of silver nanoplatelets in water near in-plane dipole resonance.

Fig. L.8.1 shows a typical transient response of the metal nanoparticle in water. The transmission (T) of the sample increases with the arrival of the pump pulse and peaks at around 370 fs delay between pump and probe. In subsequent time the transimitivity of the colloid reduces. The peak change in the absorption of the sample was estimated from the peak change in transimitivity. Fig. L.8.2 shows the intensity dependence of the peak change in the absorption of the sample for various volume fractions of silver in water. The increases with the increase in intensity of the pump pulse. However, at higher intensities tend to saturate showing the effect of fifth-order nonlinearity. Further, with increase in volume fraction of silver the change in absorption of the sample increases.

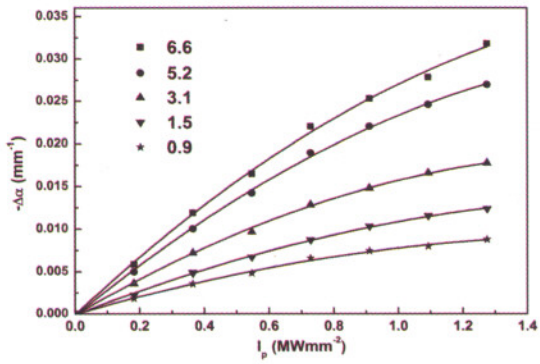

Fig. L.8.2. The change in the absorption of the sample for different pump intensities. Legend shows the volume fraction of the sample in units of 10^{-6}.

In Fig. L.8.3 we show the estimated imaginary part of third-and fifth-order nonlinearity of the silver nanoplatelets in water. Effect of pump depletion in the sample has been taken into account to correctly estimate the nonlinearities of the sample.

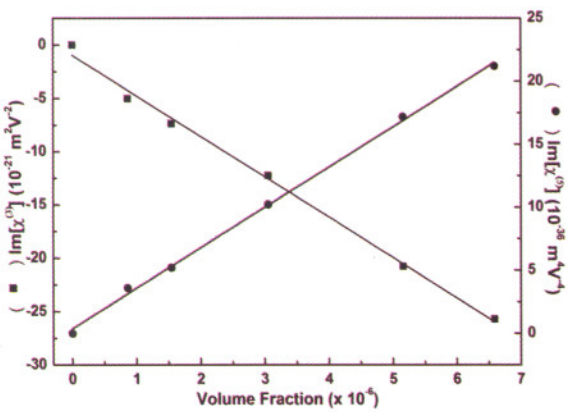

Fig. L.8.3. The dependence of third- and fifth-order nonlinearities of silver nanoplatelets in water with its volume fraction. The solid lines are the linear fit to the data.

Our results show that in low volume fractions both third- and fifth-order nonlinearities of nanoplatelets measured near one of its LSPR peak depends linearly on the volume fraction. These results are important to understand the transient nonlinear response of nonspherical nanoparticles.

Reported by:
J. Jayabalan (jjaya@rrcat.gov.in)
Asha Singh and Rama Chari

L.9: Development of a sensitive and high dynamic range laser energy meter

A sensitive and high dynamic range photo diode based laser energy meter was developed in Laser Physics Applications Division of RRCAT. The essential blocks of the energy meter are the photo detector circuit, the signal conditioning circuit and the capacitor discharge circuit. The photodiode converts the incident laser pulse into an electrical current pulse. This pulse current charge an energy sensing capacitor connected in series with the photodiode. The magnitude of the energy sensing capacitors 470 nf, 47 nf, 4.7 nf and 4.7 pf, are selected manually by a rotary switch depending on the input energy of the laser. A large resistor of 1 MΩ is connected in parallel with the energy sensing capacitor for low droop rate. For the input energy of about 12 μJ, the energy sensing capacitor of 470 nf was selected. The lowest value of the energy sensing capacitor of 4.7 pf was selected to measure the energy in the range of nJ. The signal pulse obtained with 4.7 pf was further amplified by an instrumentation amplifier AD524 to detect even the lower laser energy signals. The gain of the instrumentation amplifier can be selected from 1× to 1000× in steps of ten by a PCB mounted DIP switch. The energy meter requires ±15 V for its operation. Minimum energy of a few pJ is measured with the combination of an energy sensing capacitor of 4.7 pf and a gain of 1000 from AD524.

The signal conditioning circuit provides the buffer and the gain to the signal pulse obtained from the photo detector circuit. The output electrical pulse from the photo detector circuit was buffered by an operational amplifier buffer LF356 and was fed into the instrumentation amplifier AD524. The output of the instrumentation amplifier was buffered by an operational amplifier buffer LF356. The output voltage pulse from this buffer was measured on a Tektronix TDS2024B oscilloscope. The peak of this pulse was proportional to the incident laser pulse energy.

The long discharge time constant of the energy sensing capacitor limits the measurement of energy of the laser pulses at high repetition rate. The fast capacitor discharge circuit is therefore incorporated. A toggle switch in the signal conditioning circuit was kept 'ON' to enable the capacitor discharge circuit. The capacitor discharge circuit comprised of IC's, comparator LM311, monostable multivibrator 4047, buffer 4050 and a reed relay. It may be noted that the normally open contact of the relay is connected in parallel with energy sensing capacitor through a 100 Ω resistor. The output from the signal conditioning unit buffer was applied to the inverting input of the comparator. The other input to the comparator was kept at 60 mV dc, to avoid a possible comparator output due to noise. As soon as the photo detector output signal at the inverting input of the comparator crosses 60 mV, the comparator output changes from high to low. This eventually